A gadolinium(III) Complex Based on Pyridoxine Molecule with Single-Ion Magnet and Magnetic Resonance Imaging Properties

Marta Orts-Arroyo , Amadeo Ten-Esteve , Sonia Ginés-Cárdenas , Leonor Cerda-Alberich , Luis Marti-Bonmati , José Martínez-Lillo *

Posted Date: 17 January 2024

doi: 10.20944/preprints202401.1260.v1

Keywords: gadolinium; vitamin B6; single-ion magnet; magnetic resonance; contrast agent; relaxivity

Article

A Gadolinium(III) Complex Based on Pyridoxine Molecule with Single-Ion Magnet and Magnetic Resonance Imaging Properties

Marta Orts-Arroyo [1], Amadeo Ten-Esteve [2], Sonia Ginés-Cárdenas [2], Leonor Cerdá Alberich [2], Luis Martí-Bonmatí [2] and José Martínez-Lillo [1,*]

[1] Departament de Química Inorgànica / Instituto de Ciencia Molecular (ICMol), Universitat de València, c/ Catedrático José Beltrán 2, Paterna, 46980 València, Spain; e-mail: marta.orts-arroyo@uv.es (M.O.-A)

[2] Radiology Department and Biomedical Imaging Research Group (GIBI230), La Fe University and Polytechnic Hospital and La Fe Health Research Institute, Valencia, Spain; e-mail: amadeo_ten@iislafe.es (A.T.-E.); soniagibi230@gmail.com (S.G.-C.); leonor_cerda@iislafe.es (L.C.-A.); luis_marti@iislafe.es (L.M.-B.)

* Correspondence: f.jose.martinez@uv.es; Tel.: +34-9635-44460

Abstract: Pyridoxine is a versatile molecule that forms part of the family of B vitamins. It is used to treat and prevent vitamin B_6 deficiency and certain type of metabolic disorders. Besides, pyridoxine molecule has been investigated as a suitable ligand toward metal ions. Nevertheless, the study of the magnetic properties of metal complexes containing lanthanide(III) ions and this biomolecule has been unexplored. We have synthesized and characterized a novel pyridoxine-based Gd^{III} complex of formula $[Gd^{III}(pyr)_2(H_2O)_4]Cl_3 \cdot 2\ H_2O$ (**1**) [pyr = pyridoxine]. **1** crystallizes in the triclinic system and space group $P\bar{1}$. In its crystal packing, cationic $[Gd(pyr)_2(H_2O)_4]^{3+}$ entities are connected through H-bonding interactions involving non-coordinating water molecules and chloride anions. In addition, Hirshfeld surfaces of **1** were calculated to further investigate their intermolecular interactions in the crystal lattice. Our investigation of the magnetic properties of **1**, through ac magnetic susceptibility measurements, reveals the occurrence of slow relaxation of magnetization in this mononuclear Gd^{III} complex, this fact indicating an unusual single-ion magnet (SIM) behavior for this pseudo-isotropic metal ion at very low temperature. We have also studied the relaxometric properties of **1**, as a potential contrast agent for high-field magnetic resonance imaging (MRI), from solutions of **1** prepared in physiological serum (0.0 - 3.2 mM range) and measured at 3 T on a clinical MRI scanner. The values of relaxivity obtained for **1** are larger than those of some commercial MRI contrast agents based on mononuclear Gd^{III} systems.

Keywords: gadolinium; vitamin B_6; single-ion magnet; magnetic resonance; contrast agent; relaxivity

1. Introduction

Pyridoxine is one of the most common active forms or vitamers of vitamin B_6, which is an enzymatic co-factor involved in more than one hundred metabolic reactions, including carbohydrate, amino acid, and lipid metabolism in humans [1]. This molecule is necessary for normal brain function, given that it actively aids in producing neurotransmitters such as dopamine, serotonin, norepinephrine and gamma-aminobutyric acid [2–5]. Vitamin B_6 deficiency is associated with depression, convulsive seizures, mild microcytic hypochromic anemia, and calcium oxalate nephropathy [6].

During more than four decades, pyridoxine has also been investigated as a suitable ligand toward the preparation of metal complexes. Its pyridinic nitrogen atom and alcohols groups have been used to coordinate several metal ions (Scheme 1), such as Cd^{II} [7], Fe^{III} [8], Co^{III} [9], Cu^{II} [9–11], Sn^{IV} [12–14] and U^{VI} [15], among others [16–20]. In most cases, pyridoxine molecule is chelating or bridging through its alcohols groups, in form of alkoxide, phenolate or just as alcohol functional

 doi:10.20944/preprints202401.1260.v1

groups, and only in a few systems the pyridinic nitrogen atom is involved in the metal coordination [20–23]. From all this family of pyridoxine-based complexes, only a couple of systems have been investigated regarding their magnetic properties [18]. Concerning Gd^{III} ion, there only exists one Gd^{III} complex based on pyridoxine which has been reported in the literature [24]. This compound, of formula $[Gd^{III}(pyr)_2(NO_3)_2(H_2O)](NO_3)$, binds circulating tumor DNA (ctDNA) with a moderate affinity [24]. Nevertheless, no magneto-structural study on a pyridoxine-based Gd^{III} complex has been reported up to date.

In comparison with other lanthanide(III) complexes, the magnetic properties of Gd^{III} complexes have been much less investigated, given that Gd^{III} ion is considered magnetically isotropic because of its half-occupied $4f^7$ electron configuration (S = 7/2) and the lack of orbital contribution (L = 0) [25,26]. Hence, the number of reported homometallic Gd^{III} complexes exhibiting slow relaxation of magnetization and single-molecule/ion magnet (SMM/SIM) behavior is scarce [26–28].

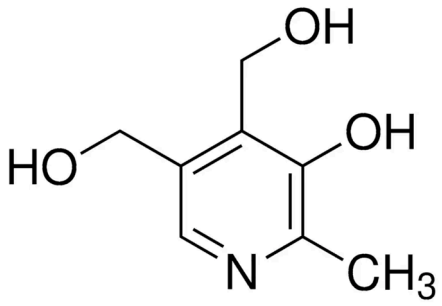

Scheme 1. Molecular structure of pyridoxine (pyr).

On the other hand, Gd^{III} metal ion is also employed as a contrast agent in magnetic resonance imaging (MRI), to improve the lesion detection and characterization, finally increasing the efficacy of diagnostic MR scans, given that Gd^{III} ion promotes changes in the relaxivity of protons from associated coordination water molecules and generates a signal with clearer physical distinction among the contrast agent and the surrounding tissues. Thus, Gd^{III}-based contrast agents have revolutionized modern technological advances in radiological diagnostics [29]. Nevertheless, novel Gd^{III}-based contrast agents are being investigated to improve the response of the current 3 T scanner devices [29,30].

It is well known that the human body uses vitamin B_6 in the metabolism. So that, it would be very interesting to obtain a complex based on Gd^{III} and vitamin B_6, which could act as a process-specific contrast agent.

Herein, we report the synthesis, the crystal structure and the magnetic and relaxometric properties of a novel pyridoxine-based Gd^{III} compound of formula $[Gd^{III}(pyr)_2(H_2O)_4]Cl_3{\cdot}2H_2O$ (**1**) [pyr = pyridoxine]. To our knowledge, **1** constitutes the first example of gadolinium-based single-ion magnet (SIM), whose study on its magnetic resonance imaging properties in a 3 T scanner has been reported.

2. Results and Discussion

2.1. Description of the Crystal Structure

Compound **1** crystallizes in the triclinic system and space group Pī (Table 1). The crystal structure is made up of cationic mononuclear $[Gd^{III}(pyr)_2(H_2O)_4]^{3+}$ complexes, chloride anions and crystallization water molecules. Indeed, the asymmetric unit of **1** contains a $[Gd^{III}(pyr)_2(H_2O)_4]^{3+}$ complex, three chloride anions and two water molecules. A perspective drawing showing the cationic Gd^{III} complex in **1** is given in Figure 1. In compound **1**, the Gd^{III} metal ion is eight-coordinate and bonded to eight oxygen atoms, two oxygen atoms (O2 and O5) from alcohol groups, two oxygen atoms (O1 and O4) from phenolate groups of two pyridoxine ligands and four oxygen atoms of four water molecules (O1w-O4w) (Figure 1). Considering the Gd-O bond lengths involving alcohol

Preprints (www.preprints.org) | NOT PEER-REVIEWED | Posted: 17 January 2024 doi:10.20944/preprints202401.1260.v1

groups, they show an average value of 2.360(1) Å, which is somewhat shorter than that of the Gd-O bond lengths of water molecules [2.424(1) Å] (Table S1).

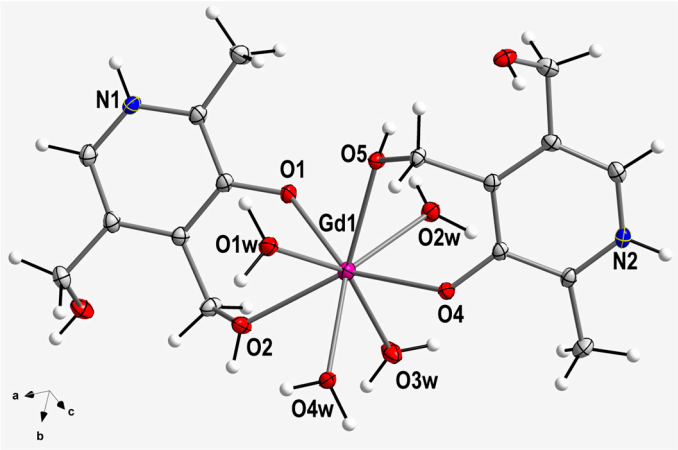

Figure 1. Perspective view of the cationic $[Gd(pyr)_2(H_2O)_4]^{3+}$ unit displaying the atom numbering scheme in **1**. Thermal ellipsoids are drawn at 50% probability level. Chloride anions and non-coordinated water molecules are omitted for clarity.

The O-Gd-O bond angles present values which cover a range from 69.13(4) to 148.95(4)°. In **1**, the two pyridine rings are planar and form an intramolecular angle of ca. 17.7(1)°. The C–C, C–N, and C–O bond lengths agree with those found in the literature for the pyridoxine molecule coordinated to different metal ions (Table S1) [8–19]. All these crystallographic data agree with those reported for other similar compounds [27,30,31].

In the crystal of **1**, the cationic $[Gd(pyr)_2(H_2O)_4]^{3+}$ entities are connected by means of H-bonding interactions generated by coordinated-water molecules and chloride anions, thus generating a 1D motif that grows along the crystallographic a axis [O1w···Cl2a = 3.133(1) Å and O4w···Cl2a = 3.147(1) Å; (a) = x+1, y, z] (Figure 2). Additional H-bonding interactions, which are formed through coordinated-water molecules and alcohol groups of pyridoxine ligands of adjacent Gd^{III} complexes, result in a layered structure growing in the ac plane [O3···O2wb = 2.730(2) Å; (b) = -x+1, -y+2, -z] (Figure 3). The shortest intermolecular Gd···Gd separation in **1** is approximately 8.640(1) Å [Gd1···Gd1c; (c) = -x+1, -y+2, -z+1]. Finally, the -NH groups of pyridoxine molecules and chloride anions are H-bonded in the third dimension of the crystal structure of **1** [N1···Cl3d = 3.218(2) Å; (d) = x+1, y, z-1] (Table 2).

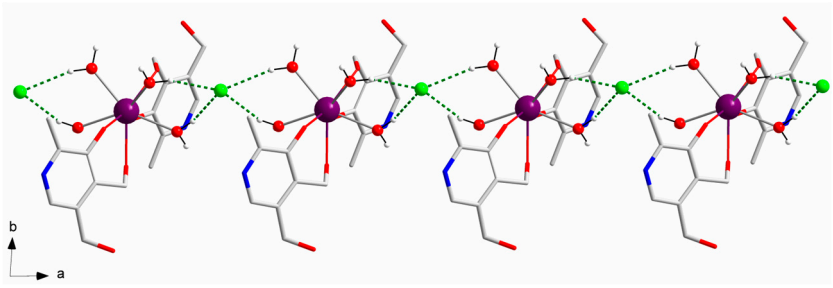

Figure 2. View of the one-dimensional motif obtained by H-bonding interactions between chloride anions and water molecules of $[Gd(pyr)_2(H_2O)_4]^{3+}$ complexes in **1**. Selected H atoms and non-coordinated water molecules are omitted for clarity. Color code: purple, Gd; green, Cl; red, O; blue, N; grey, C; white, H.

Preprints (www.preprints.org) | NOT PEER-REVIEWED | Posted: 17 January 2024 doi:10.20944/preprints202401.1260.v1

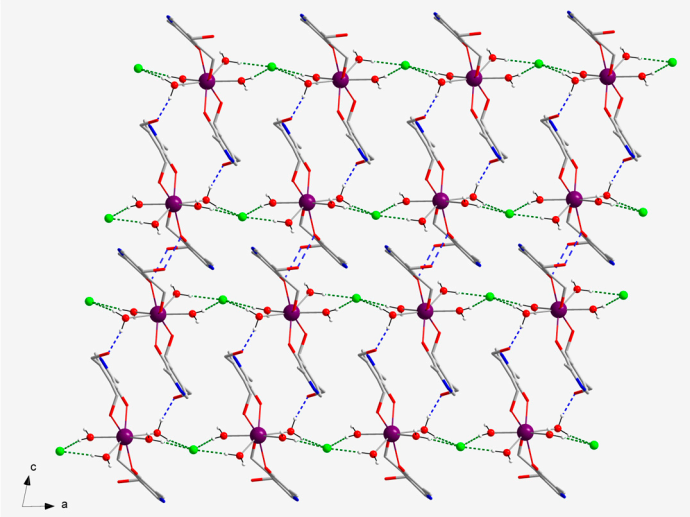

Figure 3. View of a fragment of the supramolecular 2D network generated by H-bonded O···O (dashed blue lines) and Cl···O (dashed green lines) interactions, which grow along the crystallographic ac plane in **1**. Selected H atoms and non-coordinated water molecules are omitted for clarity.

Table 1. Summary of the crystal data and structure refinement parameters for compound **1**.

Compound	**1**
CCDC	2311814
Formula	$C_{16}H_{34}N_2O_{12}Cl_3Gd$
Fw/g mol^{-1}	710.05
Crystal system	Triclinic
Space group	$P\bar{1}$
a/Å	9.042(1)
b/Å	9.323(1)
c/Å	16.265(1)
α/°	79.92(1)
β/°	76.68(1)
γ/°	84.09(1)
V/Å^3	1310.9(1)
Z	2
D_c/g cm^{-3}	1.799
μ(Mo-K$_\alpha$)/mm^{-1}	2.894
F(000)	710
Goodness-of-fit on F^2	1.068
R_1 [$I > 2\sigma(I)$]/all data	0.0174/0.0199
wR_2 [$I > 2\sigma(I)$] /all data	0.0382/0.0403

We further analyzed the coordination environment and geometry of the Gd^{III} ion in **1**. For doing that, the SHAPE program was employed. This program allows us the calculation of different polyhedra and molecular geometries for metal complexes, with the 0.000 value being the perfect match for the ideal or regular polyhedron [32]. The resulting metal symmetry can be compared with previously reported complexes and their magnetic properties [33]. In **1**, the single Gd^{III} ion displays a coordination number (CN) equal to 8. The lowest SHAPE value obtained for **1** was 0.948, which was assigned to the triangular dodecahedron geometry (TDD), the second lowest value being 1.441, which was associated with a square antiprism geometry (SAPR), see Table 3. Thus, these calculations allow us to assign the D_{2d} symmetry to the Gd^{III} metal ion in compound **1** (Table 3).

Preprints (www.preprints.org) | NOT PEER-REVIEWED | Posted: 17 January 2024 doi:10.20944/preprints202401.1260.v1

Table 2. Selected hydrogen-bonding interactions in **1**.[a]

D-H···A	D-H/Å	H···A/Å	D···A/Å	(DHA)/°
O2-H2B···O5w	0.840	1.78(1)	2.607(1)	169.0(1)
O5-H5B···Cl1	0.840	2.27(1)	3.064(1)	159.0(1)
O1w-H1wA···Cl3f	0.939	2.25(1)	3.191(1)	176.7(1)
O1w-H1wB···Cl2a	0.940	2.21(1)	3.133(1)	166.3(1)
O2w-H2wA···Cl2	0.938	2.20(1)	3.103(1)	161.0(1)
O2w-H2wB···O3b	0.943	1.80(1)	2.730(1)	169.0(1)
O3w-H3wA···Cl2	0.935	2.40(1)	3.311(1)	165.4(1)
O3w-H3wB···Cl1e	0.940	2.12(1)	3.064(1)	178.7(1)
O4w-H4wA···Cl2a	0.940	2.24(1)	3.147(1)	162.4(1)
O4w-H4wB···O6e	0.940	1.80(1)	2.743(1)	178.6(1)
O5w-H5wB···Cl3c	0.944	2.21(1)	3.146(1)	173.5(1)
O6w-H6wA···Cl3	0.948	2.16(1)	3.107(1)	174.7(1)
O6w-H6wB···Cl1g	0.943	2.25(1)	3.113(1)	152.6(1)
N1-H1A···Cl3d	0.880	2.40(1)	3.218(1)	155.3(1)
N2-H2A···O6w	0.880	1.79(1)	2.640(1)	162.7(1)
O6-H6A···O4f	0.892	1.99(1)	2.749(1)	161.2(1)
O3-H3A···Cl3h	0.888	2.39(1)	3.139(1)	159.6(1)
O5w-H5wA···Cl1e	0.955	2.25(1)	3.165(1)	159.4(1)

[a] Symmetry codes: (a) = x+1, y, z; (b) = -x+1, -y+2, -z; (c) = -x+1, -y+2, -z+1; (d) = x+1, y, z-1; (e) = x, y+1, z; (f) = -x+1, -y+1, -z+1; (g) = -x, -y+1, -z+1; (h) = x+1, y+1, z-1.

Table 3. Selected values obtained through the SHAPE program for possible geometries with coordination number (CN) equal to 8 and from the bond lengths of compound **1**.[a]

HPY	HBPY	CU	SAPR	TDD	JGBF	JETBPY	BTPR	JSD	TT
23.736	15.589	11.208	1.441	0.948	13.244	28.568	1.632	2.696	11.950

[a] Heptagonal pyramid (HPY); Hexagonal bipyramid (HBPY); Cube (CU); Square antiprism (SAPR); Triangular dodecahedron (TDD); Johnson gyrobifastigum (JGBF); Johnson elongated triangular bipyramid (JETBPY); Biaugmented trigonal prism (BTPR); Snub diphenoid (JSD); Triakis tetrahedron (TT).

2.2. Analysis of the Hirshfeld Surfaces

Intermolecular interactions involving the cationic $[Gd(pyr)_2(H_2O)_4]^{3+}$ complex of **1** were further investigated by means of CrystalExplorer program [34]. The qualitative and quantitative investigation of the main intermolecular contacts was performed by mapping the distances of the 3D surface generated considering the nearest atom outside (d_e) and inside (d_i) distances of **1** and a normalized contact distance (d_{norm}), which overcomes some limitations because of different atom sizes [35–37]. A red−white−blue set of colors is used for assigning shorter contacts (red), contacts around the van der Waals separation (white) and those longer contacts (blue) [34]. Besides, a 2D plot of the involved intermolecular interactions is generated as a fingerprint [34–37]. The Hirshfeld surface and the fingerprint plot for the cationic unit of compound **1** are given in Figure 4 and Figure S1.

The intermolecular H···Cl contacts involving mainly the coordinated water molecules, and also the -NH group of the pyridine ring of pyridoxine molecules, and chloride anions are the main interactions which are reflected on the fingerprint plot with ca. 26 % (Figure 4). An important part of these interactions are responsible for generating the 1D motifs and also the final 3D structure formed by the $[Gd(pyr)_2(H_2O)_4]^{3+}$ cations and Cl^- anions in **1**. Besides, intermolecular H···O contacts involving non-coordinated water molecules, coordinated water molecules and different protonated and deprotonated alcohol groups of pyridoxine ligands connect adjacent Gd^{III} complexes through H-bonding interactions generating a layered structure. These H···O contacts are approximately 18% of the complete fingerprint plot (Figure 4).

Preprints (www.preprints.org) | NOT PEER-REVIEWED | Posted: 17 January 2024 doi:10.20944/preprints202401.1260.v1

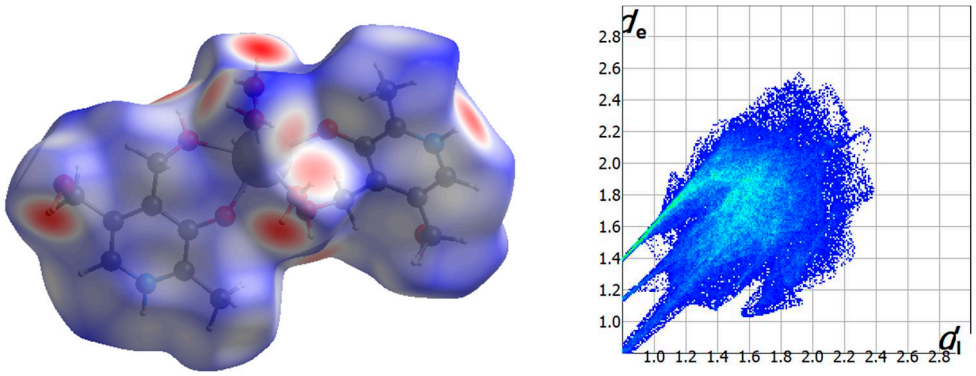

Figure 4. Hirshfeld surface mapped through d_{norm} function for the mononuclear Gd^{III} complex obtained with pyridoxine molecule in **1** (left); Full fingerprint plot for compound **1** (right).

2.3. Magnetic Properties

Direct current (dc) magnetic susceptibility measurements were performed on a microcrystalline sample of compound **1** immerse in eicosene in order to keep the sample both immobilized and well isolated from the moisture of the air at all moments. An external magnetic field of 0.5 T was applied along our temperature range (2-300 K). The experimental $\chi_M T$ vs T plot obtained for **1** is shown in Figure 5a (χ_M being the molar magnetic susceptibility per Gd^{III} ion). At room temperature, the initial $\chi_M T$ value is approximately 7.84 $cm^3mol^{-1}K$, which is just about that expected for one Gd^{III} metal ion ($4f^7$ ion with g = 2.0, S = 7/2 and L = 0) [25–28]. Upon cooling, the $\chi_M T$ value follows the Curie's law with decreasing temperature to ca. 6.0 K. After that, it slowly decreases reaching a minimum value of ca. 7.69 $cm^3mol^{-1}K$ at 2.0 K. These features presented by the dc magnetic susceptibility values, at very low temperatures, would account for intermolecular interactions and/or a very small zero-field splitting (ZFS) taking place in complex **1** [25–28].

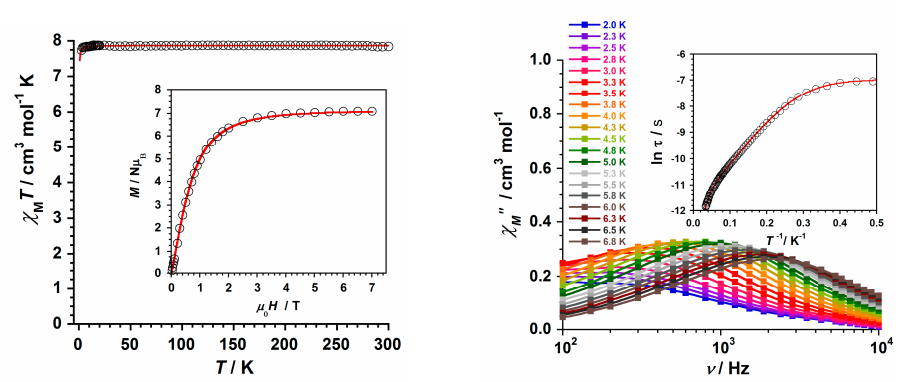

(a) (b)

Figure 5. (a) $\chi_M T$ product versus T plot for compound **1** (left), the solid red line representing the theoretical fit of the experimental magnetic susceptibility data. The inset shows the field dependence of the molar magnetization at 2.0 K (the solid red line representing the theoretical fit through the Brillouin curve generated with g = 2.0 and S = 7/2); (b) Frequency dependence of the out-of-phase ac susceptibility signals under a dc field of 2500 G for **1**. The inset displays the ln(τ) vs 1/T plot with the fit considering the contribution of two Orbach + quantum tunnelling of magnetization (QTM) mechanisms.

The field dependence of the molar magnetization (M) plot for **1** is shown in the inset of Figure 5a. The experimental M values display a continuous increase with the applied magnetic field at 2.0 K and they follow the Brillouin curve obtained with g and S values of 2.0 and 7/2, respectively (Figure 5a). The largest M value for **1** is ca. 7.07 μ_B, which agree with those of similar compounds formed by mononuclear Gd^{III} entities [25,26].

Preprints (www.preprints.org) | NOT PEER-REVIEWED | Posted: 17 January 2024 doi:10.20944/preprints202401.1260.v1

The experimental magnetic susceptibility data of the $\chi_M T$ vs T plot of **1** were analyzed by means of the theoretical equation for the magnetic susceptibility of an isotropic S = 7/2 metal ion. In addition, a θ parameter to account for possible intermolecular interactions was included [$\chi_M = (N\mu_B^2 g^2/3k_B)S(S + 1)/(T - \theta)$] [30]. Thus, the best least-squares fit gave us the following values: g = 2.005(1) and θ = −0.034(2) K with R = 5.3 × 10^{-5} for **1** {R being the agreement factor defined as $\Sigma_i[(\chi_M T)_i^{obs} - (\chi_M T)_i^{calcd}]^2/[(\chi_M T)_i^{obs}]^2$}.

Besides, alternating current (ac) magnetic susceptibility measurements were carried out on a sample of **1** in a 5.0 G ac field oscillating at different frequencies (10^2-10^4 Hz range) in the temperature range of 2.0–7.0 K. No slow relaxation of the magnetization was observed for the sample of **1** at H_{dc} = 0 G. However, out-of-phase ac signals (χ''_M) were detected when an external dc magnetic field of 2500 G was applied on **1**, indicating a field-induced Single-Ion Magnet (SIM) behavior for this mononuclear Gd^{III} system [25]. This singular magnetic behavior of **1** was studied through its χ_M'' vs frequency (ν/Hz) plot, which is given in Figure 5b. From the measured data of the relaxation maxima in the χ_M'' vs frequency (ν/Hz) plot, it is obtained the ln(τ) vs 1/T curve, which is given in the inset of Figure 5b. The experimental data of the ln(τ) vs 1/T curve draw up to three different sections, one straight line along the ca. 0.01-0.08 K^{-1} range, followed by another one in the ca. 0.10-0.30 K^{-1} range of the high-temperature region, and another straight line along the ca. 0.40-0.50 K^{-1} range of the low-temperature region. This singular ln(τ) vs 1/T curve was fully fitted only when we considered two Orbach plus a quantum tunnelling (QTM) mechanisms for the relaxation of magnetization in **1** [$\tau_o^{-1}{}_{(1)}\exp(-U_{eff(1)}/k_B T) + \tau_o^{-1}{}_{(2)}\exp(-U_{eff(2)}/k_B T)$ + QTM]. The least-squares fit of these data led to the set of parameters: U_{eff} (1) = 63.9(1) cm^{-1}, τ_o (1) = 7.9(1) × 10^{-7} s, U_{eff} (2) = 12.0(1) cm^{-1}, τ_o (2) = 6.9(2) × 10^{-6} s and QTM = 1069(5) s^{-1} for **1**.

The relaxation dynamics that **1** exhibits as single-ion magnet (SIM) is somewhat different to those of other previously reported Gd^{III} systems, given that no Raman mechanism was extracted from the experimental ac data of **1**. Nevertheless, the reported effective energy barrier (U_{eff}) values obtained for **1** should be carefully considered as they might not correspond a priori to any excited states of the Gd^{III} ion and, hence, they would not be real U_{eff} values [26,28,33]. In any case, compound **1** is one of the few SIMs based on Gd^{III} ion reported up to date, hence, further detailed experimental and theoretical investigations carried out on this quasi-isotropic 4f metal ion will be necessary to correctly understand the relaxation dynamics of the uncommon Gd^{III}-based SIMs.

Because of their relaxometric properties, mononuclear Gd^{III} systems can be studied as contrast agents, given that the electron spin relaxation rate also contributes to the proton nuclear relaxation properties, according to the Solomon−Bloembergen−Morgan (SBM) theory [38]. Nevertheless, the electron spin relaxation that we observed for the solid sample of **1** takes place at very low temperatures, whereas the magnetic resonance studies are performed in solution and at room temperature.

2.4. MR Imaging Phantom Studies

We have also studied the relaxometric properties of **1**, as a potential contrast agent for high-field MRI [39–45]. A series of 13 samples of **1** (the concentrations ranging from 0.0 to 3.2 mM) were prepared in physiological serum and were measured on a clinical MR scanner (Achieva 3T TX, Philips Healthcare, Best, The Netherlands). These measurements were performed by placing the 13 samples (with range of pH values: 7.0-7.4) in a volumetric head eight channels SENSE coil, as previously reported [30].

The methodology was based on measuring the relaxation rate (R expressed in s^{-1}), which was obtained for each concentration by means of the computation of the corresponding relaxation time T of the studied phantoms (Figure 6).

In the case of r_1, it was obtained by calculating the T1 time from sequences with 2, 5, 10, 15, 25, and 45 flip angles, whereas r_2 and r_2* values were obtained after computing T2 and T2* relaxation times, which came from sequences with echo times indicated in Table S2.

Thus, the longitudinal relaxivity (r_1) for this compound based on pyridoxine at 3 T was determined to be 34.8 $mM^{-1}s^{-1}$, whereas the transversal relaxivities r_2 and r_2* values were 18.4 and 16.6

Preprints (www.preprints.org) | NOT PEER-REVIEWED | Posted: 17 January 2024 doi:10.20944/preprints202401.1260.v1

$mM^{-1}s^{-1}$, respectively (Figure S2). These experimental results obtained for **1** show relaxivity values which are somewhat higher than those previously reported for other of our compounds, namely, the $[Gd(thy)_2(H_2O)_6](ClO_4)_3 \cdot 2H_2O$ compound (thy = thymine), which displays r_1, r_2 and r_2^* values of 16.1, 13.5 and 14.5 $mM^{-1}s^{-1}$ at 3 T, respectively [30]. In any case, these two Gd^{III} compounds based on biomolecules exhibit relaxivity values larger than those of commercial MR imaging contrast agents, such as Gadovist, Prohance, Dotarem, Omniscan and Magnevist, among others [40–45]. These experimental features make **1** potentially useful for further MRI studies, the next step being in vitro investigations.

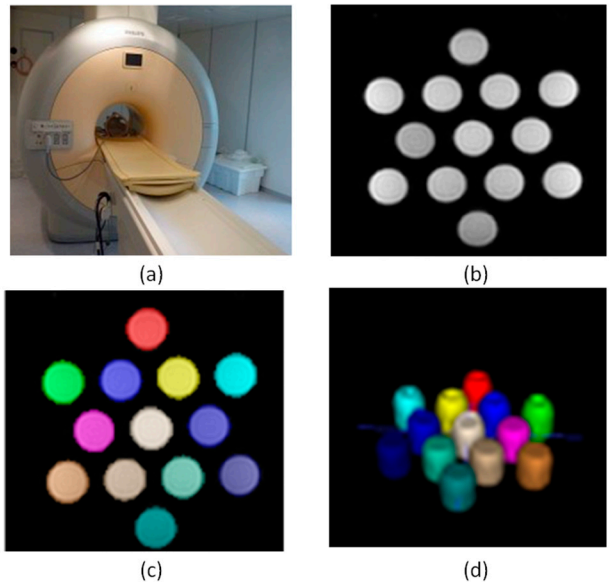

Figure 6. (a) MR imaging scanner (Philips Achieva 3T); (b) MR images of the tube phantoms containing concentrations of **1** covering the range of 0.0-3.2 mM in physiological serum, the image corresponds to the first echo of a cross section of the MEGREp sequence (Table S2); (c) Result of the automatic segmentation and labeling process of each tube on a cross section (each color corresponds to a label) of **1**; (d) Volumetric visualization of the automatic segmentation and labeling process, allowing at a quick glance to check that the tubes have been correctly identified on all cross sections.

3. Materials and Methods

3.1. Preparation of the Complex

Synthesis of 1

A mixture of $GdCl_3 \cdot 6H_2O$ (92.9 mg, 0.25 mmol) and pyridoxine (84.6 mg, 0.50 mmol) was dissolved in EtOH (3 mL) and was stirred and heated at 60 °C for 1 h. The resulting solution was filtered and then poured in a test tube and layered with n-hexane. Colorless crystals of **1** were obtained in one week and were suitable for data collection of single-crystal X-ray diffraction studies. Yield: ca. 55%. Elemental analysis calculated (found) for $C_{16}H_{34}N_2O_{12}Cl_3Gd$ (**1**): C, 27.1 (26.8); H, 4.8 (4.8); N, 3.9 (3.7)%. SEM-EDX analysis gave a Gd:Cl molar ratio of 1:3 (Figure S3). ESI-MS (m/z): 567.75 (95%). This m/z value supports the stability of complex **1** in solution (Figure S4). Selected IR data (in KBr/cm^{-1}): peaks were obtained at 3279 (s), 3172 (s), 3059 (m), 2877 (m), 2688 (m), 1617 (m), 1560 (m), 1441 (s), 1415 (m), 1352 (m), 1284 (m), 1222 (vs), 1084 (m), 1023 (vs), 984 (m), 958 (m), 885 (m), 757 (s), 694 (m), 574 (s), 519 (w), 486 (w), 417 (m) (Figure S5).

3.2. X-ray Data Collection and Structure Refinement

X-ray diffraction data collection on a single crystal of **1** of dimensions 0.14 x 0.10 x 0.05 (**1**) was collected on a Bruker D8 Venture diffractometer with PHOTON II detector at 120 K and by using Mo-

 doi:10.20944/preprints202401.1260.v1

K_α radiation (λ = 0.71073 Å). The refinement results along with crystal parameters for **1** are summarized in Table 1. The structure of **1** was solved by means of direct methods and then completed by using the SHELXTL program [46]. Then, it was refined through full-matrix least-squares refinement on F^2. Final graphical manipulations were carried out through the DIAMOND program [47]. All non-hydrogen atoms were anisotropically refined. However, the hydrogen atoms of the pyridoxine ligands were located in computed positions and refined isotropically through the riding model. Hydrogen atoms were found on all the water molecules and were fixed through DFIX. CCDC number for **1** is 2311814. These data can be obtained free of charge from the Cambridge Crystallographic Data Center on the web (http://www.ccdc.cam.ac.uk/data_request/cif).

3.3. Physical Measurements

Elemental analyses (C, H, N) were carried out in an Elemental Analyzer CE Instruments CHNS1100. The results of scanning electron microscopy (SEM-EDX) were obtained by means of a Hitachi S-4800 field emission scanning electron microscope. Electrospray Ionization Mass Spectrometry (ESI-MS) spectrum of **1** was performed on a SCIEX TripleTOF 6600+ mass spectrometer by using a direct infusion electrospray ionization source (ESI). Infrared spectrum (IR) of **1** was recorded with a PerkinElmer Spectrum 65 FT-IR spectrometer in the 4000-400 cm^{-1} region. These studies were carried out in the Central Service for the Support to Experimental Research (SCSIE) at the University of Valencia (UV). In addition, variable-temperature, solid-state (dc and ac) magnetic susceptibility data were measured on Quantum Design MPMS-XL SQUID and Physical Property Measurement System (PPMS) magnetometers at the Institute of Molecular Science (ICMol-UV). Experimental data were corrected for the diamagnetic contributions of both the sample holder and the eicosene used to immobilize the sample. Finally, the diamagnetic contribution of the involved atoms of **1** was corrected through Pascal's constants method [48].

4. Conclusions

In summary, the preparation, crystallographic studies and magnetic and relaxometric properties of a novel mononuclear Gd^{III} complex based on pyridoxine molecule and formula $[Gd^{III}(pyr)_2(H_2O)_4]Cl_3 \cdot 2\ H_2O$ (**1**) [pyr = pyridoxine] have been reported.

This compound crystallizes in the triclinic space group Pī and its crystal packing exhibits a network of H-bonding interactions involving cationic units connected through non-coordinating water molecules and chloride anions. These intermolecular interactions were further investigated by means of its Hirshfeld surfaces. In addition, selected crystal structural data were used to be computed by means of the SHAPE program, whose results account for a triangular dodecahedron geometry (TDD) and a D_{2d} symmetry assigned to the Gd^{III} metal ion in compound **1**.

The study of the magnetic properties of **1**, through both dc and ac magnetic susceptibility measurements, reveals a behavior typical of a quasi-isotropic metal ion displaying field-induced slow relaxation of magnetization and single-ion magnet (SIM) phenomenon. This magneto-structural study carried out on compound **1** is the first one performed on a lanthanide-based complex obtained with pyridoxine molecule, this fact indicating that the preparation and study of the magnetic properties of pyridoxine complexes with other more anisotropic lanthanide(III) ions, such as Tb^{III}, Dy^{III}, and Ho^{III} , could generate an interesting family of SIMs based on this versatile biomolecule. This investigation is underway in our research group.

Finally, the relaxivity properties of **1** were investigated through a preliminary study carried out by means of magnetic resonance (MR) images of the tube phantoms containing different concentrations of complex **1** prepared in physiological serum. These images were collected on a 3T clinical MRI scanner. Our results indicate that complex **1** exhibits high relaxivity values in comparison with some currently used commercial contrast agents. Hence, **1** can be considered as a potential contrast agent for high-field MR imaging and a suitable candidate for further developments and MR imaging studies on this biomedical research field.

Supplementary Materials: The following supporting information can be downloaded at the website of this paper posted on Preprints.org. Tables S1 and S2, Figures S1-S5 and CIF file of **1**.

Author Contributions: Conceptualization and funding acquisition, L.M.-B. and J.M.-L.; methodology, M.O.-A., A.T.-E., S.G.-C., L.C.-A., L.M.-B. and J.M.-L.; investigation, M.O.-A., A.T.-E., S.G.-C., L.C.-A., L.M.-B. and J.M.-L.; formal analysis, M.O.-A., A.T.-E., S.G.-C., L.C.-A., L.M.-B. and J.M.-L.; writing-original draft preparation, L.M.-B. and J.M.-L.; writing-review and editing, L.M.-B. and J.M.-L. All authors have read and agreed to the published version of the manuscript.

Funding: This research was funded by Spanish Ministry of Science and Innovation [Grant numbers PID2019-109735GB-I00 and CEX2019-000919-M (Excellence Unit "María de Maeztu")], Generalitat Valenciana [Grant number AICO/2021/295], and the VLC-BIOMED Program of the University of Valencia [Project DIGABIO PI-2020-19].

Data Availability Statement: The raw data that support the findings of this study are available from the corresponding author upon reasonable request.

Acknowledgments: The authors thank the University of Valencia for promoting calls for research programs, such as the VLC-BIOMED and similar programs.

Conflicts of Interest: The authors declare no conflict of interest.

References

1. Hellmann, H.; Mooney, S. Vitamin B6: A molecule for human health? *Molecules* **2010**, *15*, 442–459.
2. Geng, M.Y.; Saito, H.; Katsuki, H. Effects of vitamin B6 and its related compounds on survival of cultured brain neurons. *Neurosci. Res*. **1995**, *24*, 61–65.
3. Riordan, H.D.; Mikirova, N.; Taylor, P.R.; Feldkamp, C.A.; Casciari, J.J. The Effects of a Primary Nutritional Deficiency (Vitamin B Study). *Food Sci. Nutr*. **2012**, *3*, 1238–1244
4. Da Silva, V.R.; Russell, K.S.; Gregory III, J.F. Vitamin B_6. Present Knowledge in Nutrition, Tenth Edition. Wiley. Ed(s): Erdman Jr., Macdonald, I.A.; Zeisel, S.H. **2012**.
5. Parra, M.; Stahl, S.; Hellmann, H. Vitamin B_6 and Its Role in Cell Metabolism and Physiology. *Cells* **2018**, *7*, 84.
6. Percudani, R.; Peracchi, A. The B6 database: a tool for the description and classification of vitamin B6-dependent enzymatic activities and of the corresponding protein families. *BMC Bioinformatics* **2009**, *10*, 273.
7. Mosset, A.; Nepveu-Juras, F.; Harpin, R.; Bonnet, J.-J. Complexation of the vitamin B6 with the Cd^{2+} cation: NMR and X-ray structural study. *J. Inorg. Nucl. Chem*. **1978**, *40*, 1259–1263.
8. Sabirov, V.Kh.; Porai-Koshitz, M.A.; Struchkov, Y.T. Structure of the dimeric complex of iron(III) chloride with pyridoxine. *Acta Cryst.* **1993**, *C49*, 1611–1614.
9. Sudhakara Rao, S.P.; Varughese, K.I.; Manohar, H. Ternary metal complexes of anionic and neutral pyridoxine (vitamin B6) with 2,2'-bipyridine. Syntheses and x-ray structures of (pyridoxinato)bis(2,2'-bipyridyl)cobalt(III) perchlorate and chloro(2,2'-bipyridyl)(pyridoxine)copper(II) perchlorate hydrate. *Inorg. Chem*. **1986**, *25*, 734–740.
10. Mathews, I.I.; Manohar, H. Crystallographic identification of a 'stepped-cubane' structure for the Cu_4O_4 core in $[Cu_4L_2(bipy)_4(\mu_3\text{-}OH)_2][ClO_4]_4$(HL = 5-hydroxy-6-methylpyridine-3,4-dimethanol, bipy = 2,2′-bipyridine). *J. Chem. Soc., Dalton Trans*. **1991**, 2139–2143.
11. Mathews, I.I.; Sudhakara Rao, S.P.; Nethaji, N. X-ray crystal structure of a ternary copper(II) vitamin B6 complex, hydroxo(2,2′-bipyridyl)(pyridoxinato) copper(II) monohydrate. A rare example of monodentate coordination of copper(II) by the hydroxyl ion. *Polyhedron* **1992**, *11*, 1397–1401.
12. Casas, J.S.; Castellano, E.E.; Condori, F.; Couce, M.D.; Sanchez, A.; Sordo, J.; Varela, J.M.; Zuckerman-Schpector, J. Synthesis of complexes of dimethyltin(IV) with mono- and di-deprotonated pyridoxine (PN) in media with various anions. Crystal structures of $[SnMe_2(PN–H)]NO_3{\cdot}2H_2O$, $[SnMe_2(H_2O)(PN–H)]Cl{\cdot}H_2O$ and $[SnMe_2(H_2O)(PN–2H)]{\cdot}0.5H_2O$. *J. Chem. Soc., Dalton Trans.* **1997**, 4421–4430.
13. Casas, J.S.; Castiñeiras, A.; Condori, F.; Couce, M.D.; Russo, U.; Sanchez, A.; Sordo, J.; Varela, J.M. Reaction of the diethyltin(IV) cation with pyridoxine (PN, vitamin B6) in the presence of various anionic species: the crystal structure of $[SnEt_2(PN–H)]Cl$. *Polyhedron* **2000**, *19*, 813–819.
14. Casas, J.S.; Castiñeiras, A.; Condori, F.; Couce, M.D.; Russo, U.; Sánchez, A.; Sordo, J.; Varela, J.M.; Vázquez-López, E.M. Diorganotin(IV) complexes of dideprotonated pyridoxine (PN, vitamin B6). The crystal

structures of [$SnEt_2$(PN-2H)]·CH_3OH, [$SnEt_2$(PN-2H)(DMSO)] and [$SnBu_2$(PN-2H)]. *J. Organomet. Chem.* **2004**, *689*, 620–626.

15. Bonfada, E.; de Oliveira, G.M.; Back, D.F.; Lang, E.S. Metallation of Ligands with Biological Activity: Synthesis and X-Ray Characterization of [UO_2(PN)$_2$(H_2O)]Cl_2 {PN = vitamin B6 pyridoxine[2-methyl-3-hydroxy-4, 5-bis(hydroxymethyl) pyridine]}. *Z. Anorg. Allg. Chem.* **2005**, *631*, 878–881.
16. Casas, J.S.; Couce, M.D.; Sánchez, A.; Sordo, J.; Vázquez-López, E.M. Synthesis, structure and cytotoxicity studies on diorganotin (R = Me, Et) complexes of N-methylpyridoxine (MePN, PN = Vitamin B6) containing different anions. *J. Organomet. Chem.* **2012**, *696*, 4236–4247.
17. Casas, J.S.; Couce, M.D.; Sánchez, A.; Sordo, J.; Vázquez-López, E.M. Hydrogen bonded water–halide {[(H_2O)$_4$$X_2$]$^{2-}$}$_n$ (X = Cl, Br) tapes as organizing units in crystals containing [$SnMe_2$(MePN–H)]$^{2+}_2$ cations (MePN = N-methylpyridoxine). *Inorg. Chem. Commun.* **2013**, *30*, 156–158.
18. Marino, N.; Armentano, D.; Mastropietro, T.F.; Julve, M.; De Munno, G.; Martínez-Lillo, J. Cubane-Type Cu^{II}_4 and $Mn^{II}_2Mn^{III}_2$ Complexes Based on Pyridoxine: A Versatile Ligand for Metal Assembling. *Inorg. Chem.* **2013**, *52*, 11934–11943.
19. Ogryzek, M.; Chylewska, A.; Marek, P.H.; Madura, I.D.; Chmurzynski, L.; Makowski, M. Stable cationic coordination polymers of the Cu(II)-vitamin B6 type: Structural analysis, application abilities and physicochemical properties in the solid state and solutions. *Dyes Pigm.* **2017**, *136*, 278–291.
20. Chamayou, A.-C.; Neelakantan, M.A.; Thalamuthu, S.; Janiak, C. The first vitamin B6 zinc complex, pyridoxinato-zinc acetate: A 1D coordination polymer with polar packing through strong inter-chain hydrogen bonding. *Inorg. Chim. Acta* **2011**, *365*, 447-450.
21. Makhyoun, M.A.; Al-Salem, N.A.; El-Ezaby, M.S. Complexes of vitamin B6. XVII. Crystal structure and molecular orbital calculations of the dichloro-bis-pyridoxol palladium(II) complex. *Inorg. Chim. Acta*. **1986**, *123*, 117–125.
22. Acquaye, J.H.K.A.; Richardson, M.F. Palladium and platinum complexes with vitamin B6 compounds. *Inorg. Chim. Acta* **1992**, *201*, 101–107.
23. Dey, S.; Banerjee, P.; Gangopadhyay, S.; Vojtisek, P. Mixed ligand palladium(II) complexes of oxalate and malonate with vitamin-B6 molecules: synthesis, crystal structure and kinetics. *Transition Met. Chem.* **2003**, *28*, 765–771.
24. Stouder, C.E.; Warren, K.J.; Perdue, O.F.; Stewart, A.L.; Saha, A. Synthesis, characterization, computational study, and biological relevance of a family of isostructural, mononuclear Ln (Ln = Gd, Tb, Dy, Ho, Er) complexes containing pyridoxine, an essential ingredient of vitamin B6 enzyme. *Inorg. Chim. Acta* **2017**, *464*, 172–181.
25. Chen, Y.-C.; Peng, Y.-Y.; Liu, J.-L.; Tong, M.-L. Field-induced slow magnetic relaxation in a mononuclear Gd(III) complex. *Inorg. Chem. Commun.* **2019**, *107*, 107449.
26. Mayans, J.; Escuer, A. Correlating the axial Zero Field Splitting with the slow magnetic relaxation in Gd^{III} SIMs. *Chem. Commun.* **2021**, *57*, 721–724
27. Orts-Arroyo, M.; Rabelo, R.; Carrasco-Berlanga, A.; Moliner, N.; Cano, J.; Julve, M.; Lloret, F.; De Munno, G.; Ruiz-García, R.; Mayans, J.; Martínez-Lillo, J.; Castro, I. Field-induced slow magnetic relaxation and magnetocaloric effects in an oxalato-bridged gadolinium(III)-based 2D MOF. *Dalton Trans.* **2021**, *50*, 3801–3805.
28. Orts-Arroyo, M.; Sanchis-Perucho, A.; Moliner, N.; Castro, I.; Lloret, F.; Martínez-Lillo, J. One-Dimensional Gadolinium (III) Complexes Based on Alpha- and Beta-Amino Acids Exhibiting Field-Induced Slow Relaxation of Magnetization. *Inorganics* **2022**, *10*, 32.
29. Alsogati, E.; Ghandourah, H.; Bakhsh, A. Review of the Efficacy and Safety of Gadopiclenol: A Newly Emerging Gadolinium-Based Contrast Agent. *Cureus* **2023**, *15*, e43055.
30. Orts-Arroyo, M.; Ten-Esteve, A.; Ginés-Cárdenas, S.; Castro, I.; Martí-Bonmatí, L.; Martínez-Lillo, J. A Gadolinium(III) Complex Based on the Thymine Nucleobase with Properties Suitable for Magnetic Resonance Imaging. *Int. J. Mol. Sci.* **2021**, *22*, 4586.
31. Martínez-Lillo, J.; Cañadillas-Delgado, L.; Cano, J.; Lloret, F.; Julve, M.; Faus, J. A heteropentanuclear oxalato-bridged [$Re^{IV}_4Gd^{III}$] complex: synthesis, crystal structure and magnetic properties. *Chem. Commun.* **2012**, *48*, 9242-9244.
32. SHAPE 2.1, Llunell, M.; Casanova, D.; Cirera, J.; Alemany, P.; Alvarez, S. Universitat de Barcelona, Barcelona, Spain, 2013.

33. Orts-Arroyo, M.; Castro, I.; Lloret, F.; Martínez-Lillo, J. Field-induced slow relaxation of magnetisation in two one-dimensional homometallic dysprosium(III) complexes based on alpha- and beta-amino acids. *Dalton Trans*. **2020**, *49*, 9155–9163.
34. Turner, M.J.; McKinnon, J.J.; Wolff, S.K.; Grimwood, D.J.; Spackman, P.R.; Jayatilaka, D.; Spackman, M.A. CrystalExplorer 17; University of Western Australia, 2017.
35. McKinnon, J.J.; Jayatilaka, D.; Spackman, M.A. Towards quantitative analysis of intermolecular interactions with Hirshfeld surfaces. *Chem. Commun*. **2007**, 3814-3816.
36. Spackman, M.A.; Jayatilaka, D. Hirshfeld surface analysis. *CrystEngComm* **2009**, *11*, 19–32.
37. Sanchis-Perucho, A.; Orts-Arroyo, M.; Castro, I.; Lloret, F.; Martínez-Lillo, J. Crystal polymorphism in 2,2'-bipyrimidine-based iridium(III) complexes. *J. Coord. Chem*. **2022**, *75*, 2495–2507.
38. Villaraza, A.J.L.; Bumb, A.; Brechbiel, M.W. Macromolecules, Dendrimers, and Nanomaterials in Magnetic Resonance Imaging: The Interplay between Size, Function, and Pharmacokinetics. *Chem. Rev*. **2010**, *110*, 2921–2959.
39. Mousavi, B.; Chauvin, A.-S.; Moriggi, L.; Helm, L. Carbazole as linker for dinuclear gadolinium-based MRI contrast agents. *Eur. J. Inorg. Chem*. **2017**, 5403–5412.
40. Rohrer, M.; Bauer, H.; Mintorovitch, J.; Requardt, M.; Weinmann, H.-J. Comparison of magnetic properties of MRI contrast media solutions at different magnetic field strengths. *Investig. Radiol*. **2005**, *40*, 715–724.
41. Caravan, P. Strategies for increasing the sensitivity of gadolinium based MRI contrast agents. *Chem. Soc. Rev*. **2006**, *35*, 512-523.
42. Werner, E.J.; Datta, A.; Jocher, Ch.J.; Raymond, K.N. High-Relaxivity MRI Contrast Agents: Where Coordination Chemistry Meets Medical Imaging. *Angew. Chem. Int. Ed*. **2008**, *47*, 8568–8580.
43. Terreno, E.; Castelli, D.D.; Viale, A.; Aime, S. Challenges for Molecular Magnetic Resonance Imaging. *Chem. Rev*. **2010**, *110*, 3019–3042.
44. Wahsner, J.; Gale, E.M.; Rodríguez-Rodríguez, A.; Caravan, P. Chemistry of MRI Contrast Agents: Current Challenges and New Frontiers. *Chem. Rev*. **2019**, *119*, 957–1057.
45. Garrido , M.D.; Puchol , N.; El Haskouri, J.; Sánchez-Royo, J.F.; Folgado, J.V.; González Marrachelli, V.; Pérez Terol, I.; Ros Lis, J.V.; Marcos, M.D.; Ruíz, R.; Beltrán, R.; Morales, J.M.; Amorós, P. High content and dispersion of Gd in bimodal porous silica: T2 contrast agents under ultra-high magnetic fields. *Micropor. Mesopor. Mat*. **2022**, *336*, 111863.
46. SHELXTL-2013/4, Bruker Analytical X-ray Instruments, Madison, WI, 2013.
47. Diamond 4.5.0, Crystal Impact GbR, CRYSTAL IMPACT, 2018.
48. Bain, G.A.; Berry, J.F. Diamagnetic Corrections and Pascal's Constants. *J. Chem. Educ*. **2008**, *85*, 532-536.